Tunable Fiber Laser Using a MEMS-Based In Plane Fabry-Pérot Filter

Jonathan Masson, Raphael St-Gelais, *Student Member, IEEE,* Alexandre Poulin, and Yves-Alain Peter, *Senior Member, IEEE*

***Abstract*—We propose a tunable erbium doped fiber laser based on a Fabry-Pérot (F-P) cavity tuned by an electrostatic actuator. The device is made of single crystalline silicon. The F-P cavity consists of two Bragg mirrors, one being displaced by a comb-drives actuator. The F-P cavity, grooves for optical fibers and electro-mechanical structure are fabricated by deep reactive ion etching on a 70 μm silicon on insulator wafer and are integrated in a ring fiber laser. The resulting tunable fiber laser has a tuning range of 35 nm in the C-band and a spectral width of less than 0.06 nm. The maximum applied voltage for full tuning of the laser is 37 V. The mechanical resonance frequency of the actuated mirror is 14.4 kHz allowing fast tuning of the laser. The maximum output power is 1.8 mW.**

***Index Terms*—Er^{3+} doped fiber, Fabry-Pérot cavity, laser, micro-electro-mechanical system (MEMS), tunable.**

I. Introduction

LARGE refractive index difference between silicon and air and low optical absorption in the telecommunication frequency range makes silicon an ideal material for optical applications. With such a large refractive index difference (3.48 for Si and 1 for air) very few periods of a Bragg grating are needed to get highly reflective broadband dielectric mirrors. By combining two of these Bragg mirrors, a Fabry-Pérot (F-P) cavity can be assembled. Recently, several applications based on in-plane F-P cavities were proposed: tunable filters [1]–[3], amplitude modulator [4], thermal-mechanical noise sensor [5], and refractive index sensor [6].

In the first part of this paper, we demonstrate a continuously tunable micro-electro-mechanical system (MEMS) F-P filter. We use a microfabrication process that allows one single lithography and etch step for the entire device fabrication. During this process, optical components, electro-mechanical parts, as well as fiber grooves needed for optical fibers alignment are fabricated. Compact filters can be designed and tuned by varying the cavity length. Wavelength tuning over 104 nm is achieved in the telecommunication C and L-bands. In the second part of this paper, we show an application of the MEMS-based tunable F-P to a continuously tunable erbium doped ring fiber laser. Wavelength tuning over 35 nm is achieved in the telecommunication C-band.

Fiber lasers are well known and widely used in industry because of their high power and relative simplicity. They find applications as industrial cutting or welding tools [7]. Tunable fiber lasers are also good candidates as test and measurement sources for optical devices characterization because of their small spectral width, continuous tuning, and stability [8]. Wide band gain of erbium enables tuning of Er^{3+} fiber laser over the whole telecommunication C and L-bands [9]. Moreover, large Er^{3+} gain offers the opportunity to build powerful lasers or to use lossy photonic components in the laser cavity for tuning purposes [10].

Tunable fiber lasers using different strategies have been reported previously [8], [11]–[18]. For example, tunable fiber Bragg gratings [11]–[13], [15], tunable etalons [14], [17], polarization controllers [16], and thin film filters [8] were used. The pitch of fiber Bragg gratings can be tuned either by mechanical stretching [11], [12] or heating [13]. The resulting tuning range is however very limited and the tuning mechanism is usually slow. Therefore, several different Bragg gratings are needed to increase the tuning range of the fiber laser leading to a more complicated setup that includes optical switches and circulators. Tunable etalons are external cavity components requiring complicated alignment systems and are temperature sensitive [14]. Polarization controllers exhibit limited tuning range and are difficult to integrate. In this paper, the fiber laser is tuned by a MEMS F-P cavity actuated by an electrostatic comb-drive. Comb-drive actuators are known to enable fast actuation and large displacements [19]. By combining MEMS actuation to silicon optical devices, we demonstrate a compact, fast, and wide range wavelength tunable fiber laser.

In the next sections, we introduce the optical and mechanical design of the device. Simulations describing the F-P behavior using the transfer matrix method and a gaussian beam approximation are presented. The fabrication process is detailed and optical characterizations are shown and compared to optical simulations. Finally, experimental results of the tunable filter integrated into a ring fiber laser are reported.

This paper is an extension of preliminary work published in conference proceedings [20], [21]. By comparison to the filter of [20], the tuning range is greatly increased (from

Manuscript received January 8, 2010; revised March 24, 2010; accepted April 26, 2010. Date of current version July 23, 2010.

The authors are with the Department of Engineering Physics, École Polytechnique de Montréal, Montréal, QC H3C 3A7, Canada (e-mail: jonathan.masson@polymtl.ca; raphael.st-gelais@polymtl.ca; alexandre-2.poulin@polymtl.ca; yves-alain.peter@polymtl.ca).

Color versions of one or more of the figures in this paper are available online at http://ieeexplore.ieee.org.

Digital Object Identifier 10.1109/JQE.2010.2050299

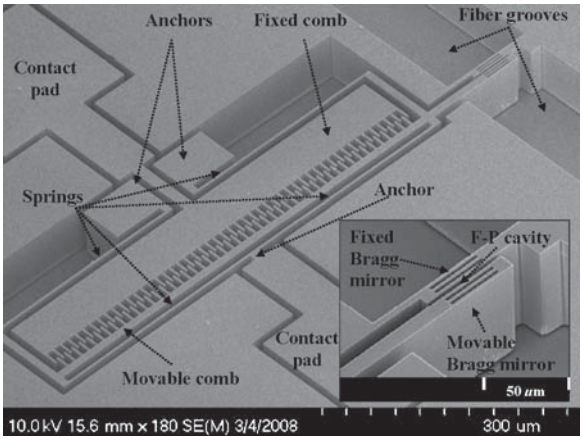

Fig. 1. Scanning electron micrograph (SEM) of the tunable filter integrated with fiber grooves and electrical contact pads. A set of four springs holds the movable comb-drive to which the movable Bragg mirror is attached.

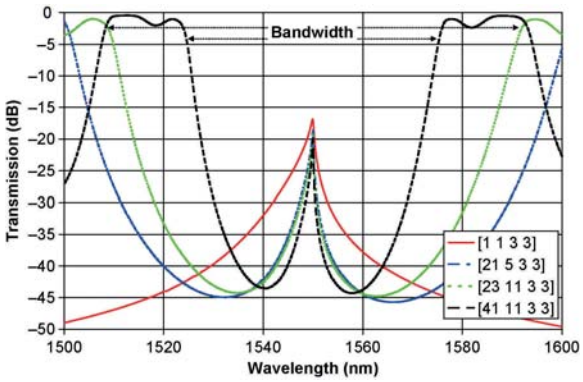

Fig. 2. Transmission spectra of four filters with different layer orders. As the order of the layers increases the transmission bandwidth decreases. The bandwidth varies from 83 nm to 52 nm when changing the silicon order from 23 to 41 with a constant air order of 11. The bandwidth is maximum when using silicon and air layers of order 1. The inset numbers correspond to [(N_{Si}) (N_{air}) (M) (number of Si walls per mirror)].

73 nm to 104 nm) and simulations are performed which allow the interpretation of the results in much greater details. By comparison to [21], the higher quality of the filter allows the tuning range of the laser to be significantly increased (from 7.7 nm to 35 nm). In fact, tuning range improvement is one of the main contribution of this paper. By comparison to the very similar filter reported in [3], the design of the MEMS actuator allows parallel displacement of the mobile mirror, which leads to a significant increase of tuning range (from 8 nm to 104 nm). The demonstration of a tunable laser would not have been possible without this novelty.

II. Device Design

Fig. 1 shows the fabricated device. The F-P filter is made of two Bragg mirrors made of alternated layers of silicon and air. The air cavity length is tuned by moving one of the Bragg mirrors using an electrostatic comb-drive actuator. The other mirror is static. The comb-drive and the movable mirror are suspended by a set of four springs. As the voltage applied to the contact pads is increased, the suspended comb is attracted toward the static one, bringing the mobile mirror toward the static one and shortening the cavity length. A smaller cavity length modifies the filter passband toward shorter wavelengths. When the voltage is decreased, the mirror goes back to its initial position (at V=0) because of the restoring force of the springs. The mechanical design of the springs and actuator is critical since the movable structure has to be highly stable to insure that the two mirrors remain parallel over the whole tuning range of the cavity. Failing to do so will generate transmission losses and broadening of the passband window. The use of a comb drive actuator suspended by four simple beam springs allows parallel displacement of the mobile mirror, which leads to an increase of the tuning range of the filter from 8 nm in [3] to 104 nm in this paper.

Light is injected and collected in and out of the filter using Corning SMF-28 optical fibers. Fibers are self-aligned on each side of the filter using fiber grooves anf spring holders. This system ensures alignment loss below 1 dB [22].

III. Simulations

Calculations based on a similar method as in [3] and [6] are used to simulate the filter behavior. The algorithm considers the divergence of the gaussian beam output from a SMF-28 optical fiber. Sources of errors such as deviation of verticality of the mirrors and surface roughness are not taken into account by the model. The transmission spectrum depends on the number of layers for each Bragg mirror and on the layer thicknesses. Fig. 2 shows typical transmission spectra for four different F-P filters made of Bragg mirrors with three silicon and two air layers, and having increasing thickness of the silicon and air layers. The thickness d of a layer is linked to the order N by $d = N\lambda/(4n)$, where N is an odd number, λ is the wavelength, and n is the refractive index of the layer. The cavity length l is given by $l = M\lambda/(2n)$, where M is the order the F-P cavity. The transmission spectrum of the F-P exhibits two side lobes, whose separation corresponds to the reflection bandwidth of the Bragg mirrors. One can see that as the mirror order increases the reflection bandwidth of the mirror gets smaller. Thus, a mirror with the largest possible reflection bandwidth should be made with layers of order 1. This is an important consideration since the reflection bandwidth is directly linked to the tuning range of the F-P by its finesse F given by $F(R) = \pi\sqrt{R(\lambda)}/(1-R(\lambda))$, where $R(\lambda)$ is the wavelength dependent reflectivity. The reflectivity is low outside the reflection bandwidth leading to a poor finesse or a poor transmission. Technology is the limit for the smallest thickness (order) that can be fabricated with conventional contact ultraviolet lithography (typically 1 μm feature size) and with a good precision (higher than 10 nm). Lipson *et al.* [3] give a detailed description on the required precision on the fabrication parameters of such filters.

The reflectivity of a Bragg mirror is directly related to the number of dielectric layers [23]. Adding layers enhances the interference effect of the dielectric Bragg mirror, thus increasing reflectivity of the mirrors. Nevertheless, many periods Bragg mirrors do not provide the optimal properties in our configuration. Indeed, optical fibers output beam waist size is

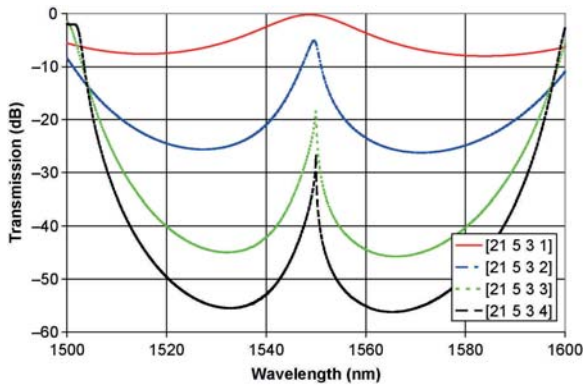

Fig. 3. Superposed transmission spectra of a simulated device having an increasing number of silicon and air layers per Bragg mirror. When the number of layers is increased, the transmitted peak is narrower but the transmission losses are higher due to the gaussian beam divergence.

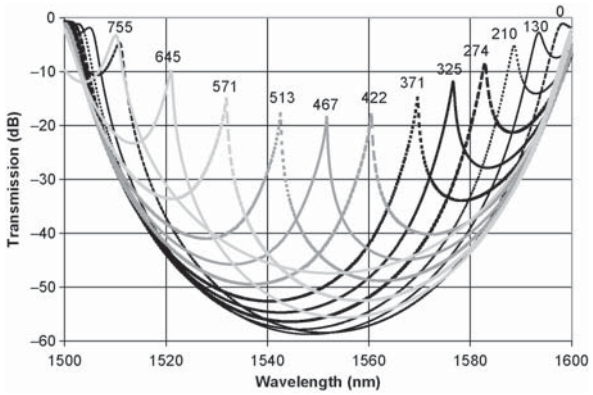

Fig. 4. Transmission spectra of a simulated device of type [21 5 3 3]. The F-P gap length is varied from 2.800 μm to 2.155 μm. The numbers over each peak correspond to the displacement of the movable mirror (in nm) from its rest position.

typically 5 μm at 1550 nm, and thus has significant divergence. Many layers Bragg mirrors are highly reflective. Therefore, the lifetime of the light in the cavity is very long and losses increase dramatically as shown in Fig. 3. Using one silicon wall per Bragg mirror the transmission is close to 0 dB, but the full width at half maximum (FWHM) of the peak is 21 nm. For three silicon walls per Bragg mirror the transmission drops to -18 dB and the FWHM to 0.6 nm. We found experimentally that the optimum number of layers per Bragg mirror is three silicon layers and two air layers. A beam expander could be used to circumvent the divergence effect.

For a wavelength of 1550 nm the thicknesses of the layers are designed to be 2.4 μm and 1.9 μm (corresponding to 21st and fifth orders) for silicon and air, respectively. Fig. 4 shows the simulated transmitted spectra of a F-P filter which is tuned by 88 nm from 1598 to 1510 nm. The inset numbers show the required displacement of the mirror (in nm) to generate the corresponding tuning. When there is no displacement the gap is 2.8 μm long and the transmission peak is located near the largest wavelengths (1600 nm). When the gap length is shortened by actuating the comb-drive the transmission peak moves toward smaller wavelength. A total displacement of 755 nm is needed to tune through the whole bandwidth of the filter. The best simulated FWHM for a transmitted peak at 1550 nm is 0.6 nm. As the peak moves closer to the bandwidth border the FWHM broadens to 2.3 nm.

IV. Fabrication

The filter is fabricated on a silicon on insulator (SOI) wafer. The device layer of the SOI is 70 μm thick and the silicon oxide sacrificial layer is 2 μm thick. A 4.2-μm-thick Shipley SPR 220 3.0 photoresist was used to sustain deep reactive ion etching (DRIE) processing. The alternate silicon and air layers of the filter are vertically etched over the 70 μm of the device layer. The U-grooves for fibers self-alignment, the springs, and the comb-drive actuator are etched simultaneously.

DRIE was realized in an Oxford Instruments Plasmalab System 100. Table I shows the etching parameters. 700 passivation and etch cycles were applied. The structure was released by etching the SiO_2 sacrificial layer using 49% concentrated liquid HF during 3 min. The anchors and the static comb are not completely released since they are much larger than the mobile structures (they stay attached to the remaining oxide). To prevent the released device from sticking to the substrate, supercritical CO_2 drying was used.

TABLE I
DRIE Parameters

Step	Passivation	Pause	Etching
ICP power (W)	450	0	450
RF power (W)	10	0	25
C_4F_8 (sccm)	65	0	1
SF_6 (sccm)	1	0	65
O_2 (sccm)	0	0	5
Time (s)	4	2	4

The inset of Fig. 1 shows the optical part of the fabricated device. A verticality of 89.5° and a surface roughness of 26.2 nm RMS were reached for the vertical walls. The surface roughness was measured by an atomic force microscope on an etched edge.

Verticality was measured using the scanning electron microscope (SEM) micrograph of a cleaved sample grating having the same dimension as the filter. It was calculated by measuring the width of the 70 μm deep trenches at the top and at the bottom of the region that is in interaction with the light beam (at trench depths of 5 μm and 15 μm). The precision of this method is relatively low (a variation of 2 nm of the measured thickness leads to a deviation of the calculated verticality of more than 0.01°). Therefore, the reported value is an upper boundary determined by repeating the measurements several times. For the experimental results of Fig. 5, it is possible that the verticality was significantly better. This could explain that good optical results are reported despite the fact that, in [3], calculations indicate that verticality better than 89.99° is required.

V. Optical Characterization

A broadband source (Newport BBS-430) was used for the optical characterization of the F-P. Light is injected into the device using an SMF-28 optical fiber aligned in the fiber

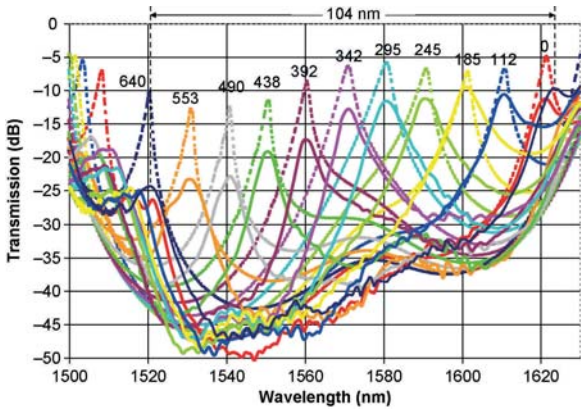

Fig. 5. Superposed transmission spectra of the F-P tuned with different voltage and the corresponding fitted simulation curves (dashed). The inset numbers show the simulated displacement in nanometers of the movable mirror to fit the experimental data.

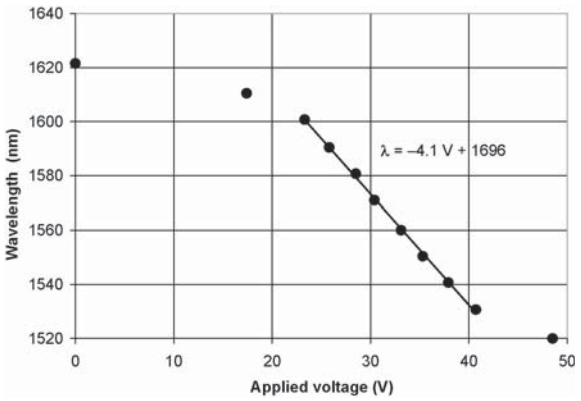

Fig. 6. Transmitted wavelength as a function of the applied voltage to the comb-drive.

groove. Another fiber is placed on the other side of the F-P to collect the transmitted light which is guided to an Agilent 86142A optical spectrum analyzer. All results presented in the following part of the paper were obtained using a filter having the configuration [21 5 3 3].

The filter is tuned by applying a voltage between the static and the movable comb using a DC voltage source. Fig. 5 shows the superposed spectra of the tuned F-P filter. The dashed curves are the simulated fit. At rest, the transmitted wavelength was 1621 nm. As we increased voltage, the transmitted peak is shifted continuously toward smaller wavelength. At a voltage of 40.7 V, the transmitted wavelength is of 1531 nm covering a tuning range of 90 nm. If the voltage is increased up to 48.5 V two transmitted peaks appear on the same curve. The separation between those peaks is the free spectral range (FSR) of the filter (104 nm). This value is the maximum tuning range of the filter. The spectral width of the filter varies between 4.4 nm and 7.6 nm and losses between −9.46 dB and −24 dB. Fig. 6 shows the transmitted wavelength as a function of applied voltage to the comb-drive. The linear part of the curve has a sensitivity of −4.1 nm/V.

The resonance frequency of the suspended structure was measured using a dynamic white light interferometer (Fogale Nanotech Photomap 3-D). The first mode appears at 14.4 kHz

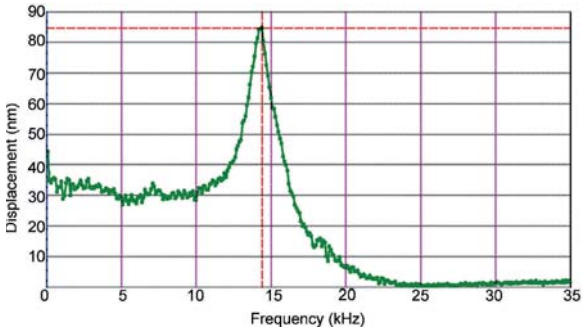

Fig. 7. Displacement amplitude of the movable mirror when an AC voltage is applied to the comb-drive. The first excitation mode resonance frequency is at 14.4 kHz.

with an in plane deformation. Fig. 7 shows the displacement of the movable mirror when an AC voltage is applied to the comb-drive actuator.

To fit the optical simulations with the experimental results, we have to take into account some fabrication imperfections. The most important one comes from the over etch caused by the DRIE. During the silicon etching process, the final thicknesses of the silicon layers are smaller than the one defined on the photomask and transferred to the photoresist. This is due to lateral under etching of the silicon by the SF_5^+ ions [24]. Recalling from the definition of the thickness d of a silicon wall to meet the Bragg condition, the thickness difference between two consecutive Bragg orders N and $N+1$ is only 112 nm. This means that an over etch of only 112 nm in a silicon layer is enough to change N from an odd to an even number. In this case, reflectivity of the Bragg mirrors drops dramatically so that the F-P performances decrease. Precise measurement and control of the over etch must be achieved to obtain good optical results. SEM photographs of a cleaved grating allowed to estimate this over etch. Using the simulation algorithm, the experimental data is fitted by varying the over etch to find its precise value. The best fit was obtained for an over etch of 710 nm per silicon layer. An over etch error on the two silicon walls facing the fiber grooves was also considered. Since these walls are exposed to a large etched area (the fiber groove), they are more exposed to ion bombardment than the inner silicon walls. As an effect, they are thinner. To have an accurate simulation, an additional 85 nm over etch was considered for these walls. Moreover, since the F-P gap is larger than the air layers of the Bragg mirrors, a larger over etch on each side of the air gap must also be taken into account. In this case, 15 nm of over etch were added in the air gap layer. The displacement of the movable Bragg mirror needed to tune the filter is finally fitted using the above-mentioned parameters. Dimensions in Fig. 5 refer to the displacement needed to tune the filter at the corresponding wavelength. A maximum experimental displacement of 629 nm is needed to tune the filter over its full range. It is close to the predicted 755 nm of displacement from the simulations (see Fig. 4).

The asymmetric shape of the reflection band of the Bragg mirrors is explained by the model and is due to the excess over etch occurring in the larger openings. For an optical cavity, the

Q factor is linked to the finesse and to the photon lifetime in the cavity t by $Q = \lambda/\text{FWHM} = F\lambda/\text{FSR} = 2\pi t\nu$, where ν is the transmitted frequency. At around 1540 nm, the reflection is at its highest value and, as demonstrated in Fig. 3, the FWHM of the peak is the smallest but, since the lifetime in the cavity is longer, divergence losses are higher.

For resonance peaks located between 1520 nm and 1545 nm, the difference between the simulated and the experimental curves increases. Again, this is related to the photon lifetime in the cavity. When it gets longer, the light interacts more with the Bragg mirrors and the losses due to imperfections which are not taken into account by the model (surface roughness, imperfect verticality) are enhanced.

In Fig. 5, it might seam contradictory that the experimental results sometimes present less loss than the simulated results of Fig. 4. The reason is that the simulations of Fig. 4 are performed for a F-P filter having exact nominal dimensions (odd multiple of a quarter of the central wavelength 1550 nm). Experimentally, this case is never reached perfectly. The experimental reflectivity of the mirrors is therefore always lower than the value of Fig. 4. For lower reflectivity, the light is less confined in the resonator and the losses due to divergence decrease. In Fig. 5, the same simulations are performed using the real dimensions of the silicon and air layers. In this case, the experimental transmission at the resonance wavelengths is never higher than the simulations.

Moreover, it should be noted that although the measured losses of Fig. 5 are sometimes less important than for the simulations of Fig. 4, the experimental finesse of the F-P resonance is never higher than expected. Again this is related to the lower reflectivity of the Bragg mirrors due to over etching. To summarize, it is not contradictory to obtain lower than expected losses since this happens at the expense of a lower finesse of the F-P.

VI. Tunable Fiber Laser

Tuning the wavelength of a laser is one interesting application for a MEMS F-P filter. By introducing the filter into a laser cavity, the emission wavelength can be tuned continuously. In this section, a MEMS-based tunable erbium doped ring fiber laser is demonstrated. A ring laser can be widely tunable, have a narrow emission spectrum and have high output power. The gain provided by the erbium doped fiber can be higher than 20 dB and it spans over the telecommunication C and L bands. In our case, this high gain is required to meet the lasing condition since the F-P filter has high optical loss. A ring fiber laser has no mirror since the light is guided in the optical fiber that is closed onto itself to form a loop. By opening the cavity and aligning the optical fibers on each side of the F-P filter, the filter is fully integrated within the cavity. Fig. 8 shows a schematic of the fiber laser setup. Light from a pump laser diode at 1480 nm is injected through a wave division multiplexing (WDM) coupler into the fiber laser cavity. Six meters of erbium doped fiber (Liekki Er30-4/125) were used. An isolator is placed to insure one way lasing direction. A polarization controller is introduced to improve the laser stability. The fiber laser is continuously tuned over 35 nm from

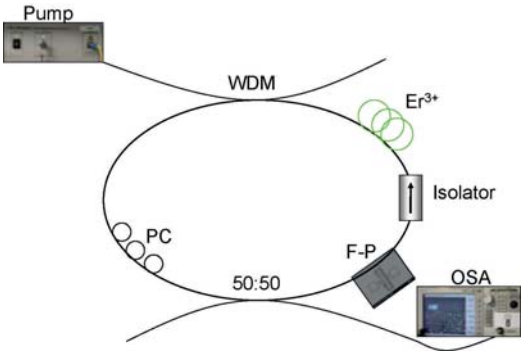

Fig. 8. Schematic setup of the ring fiber laser configuration.

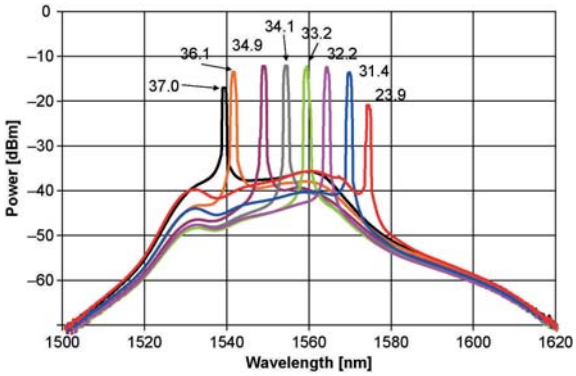

Fig. 9. Emission spectra of the tuned fiber laser. The inset numbers are the applied voltages in volts to the comb-drive to continuously tune the laser from 1539 to 1574 nm covering a range of 35 nm.

1539 nm to 1574 nm (Fig. 9). Tuning the laser is realized by tuning the F-P filter as mentioned above. Tuning is controlled by a voltage from 23.9 V to 37.0 V applied to the comb-drive actuator. Because of the high resonance frequency of the MEMS, tuning of the laser is done in tens μs. The variation of the output power across the tuning range is less than 8 dBm. The threshold of the laser is 32.6 mW of absorbed pump power and the slope efficiency is 2.14%. The low slope efficiency is due to the important transmission losses of the F-P filter. Maximal output power (1.8 mW) was obtained using a 50:50 output coupler. The theoretical longitudinal mode spacing in the 8 m long cavity is 25 MHz. The line width of the laser is formed by simultaneous laser emission of many adjacent longitudinal modes [8]. Because of these close longitudinal modes, when changing the selected wavelength with the filter, virtually continuous tuning of the laser is achieved. Even if the spectral width of the filter is relatively large the spectral width of the laser is bellow 0.06 nm (limited by the resolution bandwidth of the optical spectrum analyzer). The tuning range of the laser is limited compared to the tuning range of the filter. The tuning range of the laser is limited by the F-P filter losses, the erbium gain shape and the limited bandwidth of the WDM coupler. Because of the high losses of the filter, the lasing threshold is met only in the spectral region where the combined gain of the doped fiber and transmission of WDM coupler are maximum. Changing the pumping laser wavelength to 980 nm would allow to use a larger bandwidth

coupler increasing the tuning range. Moreover, using a longer doped fiber length could increase the optical gain in the L-band region. Optimization of the laser cavity and of the filter must be done to expand the tuning range and the output power of the laser. However, to the best of our knowledge, a tunable MEMS-based fiber laser was not demonstrated yet. It is an interesting development for fast and compact tunable fibre lasers.

VII. Conclusion

In this paper, we presented a wide range tunable filter. By using a single step etching process, a very compact and integrated tunable F-P filter was fabricated. Optical fibers, actuator, and the optical device were fabricated in one single etching step. Tuning as large as 104 nm in the optical C and L-bands was demonstrated. A mechanical resonance frequency of 14.4 kHz was measured allowing tuning over the whole dynamic range of the filter in few μs. In the second part of this paper, we presented a novel approach to tune a fiber laser with the MEMS actuated F-P filter. By introducing the MEMS F-P filter into a ring fiber laser cavity, a compact tunable fiber laser was demonstrated. The tuning range is 35 nm with a spectral width of less than 0.06 nm.

At this point, the tunable laser is still a basic proof of concept. However, since MEMS allows fast actuation and low cost batch fabrication, our technology opens the path to a wide range of applications in telecommunications, metrology, laser machining, and bio-chemical sensing using high quality integrated tunable fiber lasers.

References

[1] S.-S. Yun, K.-W. Jo, and J.-H. Lee, "Crystalline Si-based in-plane tunable Fabry-Pérot filter with wide tunable range," in *Proc. IEEE/LEOS Int. Conf. Opt. MEMS*, 2003, pp. 77–78.

[2] B. Saadany, M. Malak, M. Kubota, F. M. Marty, Y. Mita, D. Khalil, and T. Bourouina, "Free-space tunable and drop optical filters using vertical Bragg mirrors on silicon," *IEEE J. Sel. Top. Quantum Electron.*, vol. 12, no. 6, pp. 1480–1488, Nov.–Dec. 2006.

[3] A. Lipson and E. Yeatman, "A 1-D photonic band gap tunable optical filter in (110) silicon," *J. Microelectromech. Syst.*, vol. 16, no. 3, pp. 521–527, 2007.

[4] C. A. Barrios, V. R. Almeida, R. R. Panepucci, B. S. Schmidt, and M. Lipson, "Compact silicon tunable Fabry-Pérot resonator with low-power consumption," *IEEE Photon. Technol. Lett.*, vol. 16, no. 2, pp. 506–508, Feb. 2004.

[5] M. W. Pruessner, T. H. Stievater, and W. S. Rabinovich, "In-plane microelectromechanical resonator with integrated Fabry-Pérot cavity," *Appl. Phys. Lett.*, vol. 92, no. 8, p. 081101, 2008.

[6] R. St.-Gelais, J. Masson, and Y.-A. Peter, "All-silicon integrated Fabry-Pérot cavity for volume refractive index measurement in microfluidic systems," *Appl. Phys. Lett.*, vol. 94, no. 24, p. 243905, 2009.

[7] T. Hausken, "Incumbent sources resist fibre laser proliferation," *Opt. Laser Eur.*, vol. 157, pp. 31–34, Jan. 2008.

[8] A. Bellemare, M. Karbsek, C. Riviere, F. Babin, G. He, V. Roy, and G. Schinn, "A broadly tunable erbium-doped fiber ring laser: Experimentation and modeling," *IEEE J. Sel. Top. Quantum Electron.*, vol. 7, no. 1, pp. 22–29, Jan.–Feb. 2001.

[9] J. A. Buck, *Fundamentals of Optical Fibers*, 2nd ed. New York: Wiley, 2004.

[10] M. J. F. Digonnet, *Rare-Earth-Doped Fiber Lasers and Amplifiers*, 2nd ed. Boca Raton, FL: CRC Press, 2001.

[11] S.-K. Liaw, K.-L. Hung, Y.-T. Lin, C.-C. Chiang, and C.-S. Shin, "C-band continuously tunable lasers using tunable fiber Bragg gratings," *Opt. Laser Technol.*, vol. 39, no. 6, pp. 1214–1217, Sep. 2007.

[12] S. Yamashita and M. Nishihara, "Widely tunable erbium-doped fiber ring laser covering both C-band and L-band," *IEEE J. Sel. Top. Quantum Electron.*, vol. 7, no. 1, pp. 41–43, Jan.–Feb. 2001.

[13] N.-K. Chen, D.-Y. Hsu, and S. Chi, "Widely tunable asymmetric long-period fiber grating with high sensitivity using optical polymer on laser-ablated cladding," *Opt. Lett.*, vol. 32, no. 15, pp. 2082–2084, 2007.

[14] H. Y. Ryu, W.-K. Lee, H. S. Moon, and H. S. Suh, "Tunable erbium-doped fiber ring laser for applications of infrared absorption spectroscopy," *Opt. Commun.*, vol. 275, no. 2, pp. 379–384, 2007.

[15] S.-K. Liaw and G.-S. Jhong, "Tunable fiber laser using a broad-band fiber mirror and a tunable fbg as laser-cavity ends," *IEEE J. Quantum Electron.*, vol. 44, no. 6, pp. 520–527, Jun. 2008.

[16] P. Humphrey and J. Bowers, "Fiber-birefringence tuning technique for an erbium-doped fiber ring laser," *IEEE Photon. Technol. Lett.*, vol. 5, no. 1, pp. 32–34, Jan. 1993.

[17] C. Poulsen and M. Sejka, "Highly optimized tunable Er3+-doped single longitudinal mode fiber ring laser, experiment and model," *IEEE Photon. Technol. Lett.*, vol. 5, no. 6, pp. 646–648, Jun. 1993.

[18] C. H. Yeh, F. Y. Shih, C. N. Lee, C. T. Chen, and S. Chi, "Wavelength-tunable erbium fiber ring laser in single-frequency operation utilizing Fabry-Pérot laser with Sagnac cavity," *Opt. Commun.*, vol. 281, no. 9, pp. 2454–2458, 2008.

[19] C. Chen and C. Lee, "Design and modeling for comb-drive actuator with enlarged static displacement," *Sensors Actuators A*, vol. 115, nos. 2–3, pp. 530–539, 2004.

[20] J. Masson, F. B. Kone, and Y.-A. Peter, "MEMS tunable silicon Fabry-Pérot cavity," *Proc. SPIE*, vol. 6717, no. 5, 2007.

[21] J. Masson, S. Bergeron, A. Poulin, N. Godbout, and Y.-A. Peter, "Tunable erbium doped fiber laser using a silicon micro-electro-mechanical Fabry-Pérot cavity," in *Proc. IEEE/LEOS Int. Conf. Opt. MEMS Nanophoton.*, 2007, pp. 171–172.

[22] Z. F. Wang, W. Cao, and Z. Lu, "Moems: Packaging and testing," *Microsyst. Technol.*, vol. 12, nos. 1–2, pp. 52–58, 2005.

[23] R. Kashyap, *Fiber Bragg Gratings*. New York: Academic Press, 2004.

[24] H. Jansen, M. de Boer, and M. Elwenspoek, "The black silicon method VI: High aspect ratio trench etching for MEMS applications," in *Proc. Micro Electro Mech. Syst.*, 1996, pp. 250–257.

Jonathan Masson graduated with a degree in engineering physics from the École Polytechnique de Montréal (EPM), Montréal, QC, Canada, in 2006. During his studies, he made a year long exchange at the Institut National Polytechique de Grenoble, Grenoble, France. He attained his M.S. degree from the EPM working on tunable silicon grating under the supervision of Professor Yves-Alain Peter. He is currently pursuing the Ph.D. degree in the field of optical micro-electro-mechanical systems from Institute of Microengineering, Sensors, Actuators and Microsystems Laboratory, École Polytechnique Fédérale de Lausanne, Neuchâtel, Switzerland.

Raphael St-Gelais (S'08) received the B.Eng. degree in engineering physics from École Polytechnique de Montréal, Montréal, QC, Canada, in 2007. He is currently pursuing the Ph.D. degree from the same institute with the support of an Alexander Graham Bell Canada Graduate Scholarship.

He was an Engineering Intern with Dalsa Semiconductor, Bromont, QC, Canada, during a short period before joining the Micro and Nano Systems Laboratory, École Polytechnique de Montréal, in 2008. His work is published in peer-reviewed journals and international conference proceedings. His current research interests include optical microelectromechanical systems, silicon photonics, and microfluidics for applications, such as on-chip optical biosensors and tunable components for optical fiber networks.

Alexandre Poulin studied engineering physics at École Polytechnique de Montréal (EPM), Montréal, QC, Canada. While an undergraduate, he did a one-year-long international exchange to study physics at the École Polytechnique Fédérale de Lausanne, Lausanne, Switzerland. In 2009, he gained an accelerated passage to graduated studies. He is currently pursuing the Masters degree in fast micro-electro-mechanical systems tunable lasers from EPM, under the supervision of Professor Yves-Alain Peter.

Yves-Alain Peter (S'93–M'03–SM'07) received the M.S. degree in physics and the Dr.Sc. degree in sciences from the University of Neuchâtel, Neuchâtel, Switzerland, in 1994 and 2001, respectively.

In 1995, he was a Research Associate with the Medical Radiobiology Department, Paul Scherrer Institute, Villigen, Switzerland. From 1995 to 2001, he was a Graduate Research Assistant with the Applied Optics Group, Institute of Microtechnology, University of Neuchâtel. From 2001 to 2003, he was a Post-Doctoral Researcher with the Microphotonics Group, Stanford University, Stanford, CA. From 2003 to 2004, he was a Research and Development Engineer and Project Leader with the Swiss Center for Electronics and Microtechnology, Neuchâtel, Switzerland. He is currently an Associate Professor and the Deputy Director of the Thin Film Research Laboratories, Department of Engineering Physics, École Polytechnique de Montréal, Montréal, QC, Canada. His current research interests include microoptoelectromechanical systems, optical microcavities, and tunable nanophotonics structures.

Dr. Peter has held several positions on various program committees and reviews, including the Program Chair of the 2008 IEEE Photonics Society Optical Microelectromechanical Systems and Nanophotonics Conference, and the Primary Guest Editor of the IEEE JOURNAL OF SELECTED TOPICS IN QUANTUM ELECTRONICS special issue on "Nanophotonics and Optical MEMS" (vol. 15, no. 5, 2009). He is a member of the IEEE Photonics, the Optical Society of America, and the Swiss Physical Society.